Optics Letters

Temperature distribution inversion in infrared multispectral imaging based on ensemble network

Shuowen Yang,[1] Hanlin Qin,[1,*] Yang Dai,[1] Xiang Yan,[1] and Ana Belén López-Baldomero[2]

[1]School of Optoelectronic Engineering, Xidian University, Xi'an 710071, China
[2]Department of Optics, Faculty of Sciences, University of Granada, Granada 18071, Spain
*hlqin@mail.xidian.edu.cn

Received 24 June 2024; revised 14 August 2024; accepted 16 August 2024; posted 16 August 2024; published 6 September 2024

Temperature distribution can be acquired through non-contact temperature measurement using multispectral imaging. However, the challenge lies in radiometric temperature inversion owing to the unknown emissivity. Despite the promising results demonstrated by traditional algorithms and neural networks, enhancing the precision and reliability of temperature inversion remains a challenge. To tackle these challenges, in this work, we propose the use of ensemble learning for temperature distribution inversion in infrared multispectral imaging. The network comprises a base-learner and a meta-learner, trained to establish the nonlinear relationship between temperature and multispectral distribution measurements. Moreover, the network architecture exhibits high robustness against noise arising in the testing environment. Simulations and real experiments on multispectral imaging measurements illustrate that ensemble learning can be a potent tool for multispectral imaging radiation temperature distribution measurement, achieving superior inversion performance compared to other neural networks. The reproducible code will be available at https://github.com/shuowenyang/Temperature-Inversion.

https://doi.org/10.1364/OL.533666

Introduction. Multispectral pyrometry offers the benefits of rapid response, non-contact measurement, and absence of an upper-temperature limit [1,2]. Nevertheless, the majority of pyrometers focus on single-point measurements, often falling short in accurately capturing temperature within regions of interest (ROI). Multispectral imaging expands temperature measurement to encompass distribution, showing promising applications across diverse fields, such as temperature monitoring in petroleum refining industry, transportation, defense, and aerospace industries [3,4]. Temperature inversion is typically achieved through spectral measurement of objects, whose emissions strongly correlate with temperature. However, the lack of emissivity information of objects poses a challenge to recover temperature distributions accurately.

For multispectral measurement of i spectral channel, mathematically, the temperature model can be represented as follows:

$$\frac{V_i}{\hat{V}_i} = \epsilon(\lambda_i, T) \cdot e^{-\frac{C_2}{\lambda_i T}} \cdot e^{-\frac{C_2}{\lambda_i T'}} \tag{1}$$

where V_i denotes the output signal from the i-th spectral channel of target. $\hat{V}_i$ represents the acquisition signal of the blackbody from the i-th spectral channel. $\epsilon(\lambda_i, T)$ is the target spectral emissivity at temperature T, T' denotes the reference temperature of the blackbody, and C_2 denotes the second radiation constant. However, solving Eq. (1) presents an inverse problem as the number of unknowns exceeds the number of equations. A feasible solution involves predefining a specific relationship between emissivity and wavelength. Sun *et al.* [5] developed a quadratic measurement method based on the temperature–emissivity model for inversion. Xing *et al.* [6] proposed a quadratic measurement method under the assumption of a linear relationship between emissivity and temperature across different wavelengths. However, emissivity does not consistently change linearly with temperature in all cases. Therefore, this hypothesis lacks robustness, constraining the accurate inversion of real-world situations. An alternative approach to address this issue is to reformulate the inversion problem as an optimization problem, imposing constraints to restrict the number of solutions. Xing *et al.* [7] utilized gradient projection and applied a penalty function for optimization. Subsequently, Zhao *et al.* [8] introduced the improved grey wolf optimization (IGWO) algorithm, enabling the simultaneous estimation of temperature and emissivity without relying on an emissivity hypothesis model. Although not requiring an emissivity hypothesis model, these methods suffer from low computational efficiency due to their iterative procedure.

Recently, neural networks have demonstrated the potential to solve inverse problems. Unlike traditional optimization methods, neural networks treat this inverse problem as a nonlinear mapping. Rather than relying on hypothesis models, Cong *et al.* [9] utilized a radial basis function (RBF) network to simulate the emissivity model, enabling multispectral radiometric temperature measurement. Additionally, Sun *et al.* [10] introduced a genetic algorithm combined with a neural network for temperature inversion. Inspired by backpropagation (BP) networks, Gao *et al.* [11] devised an emissivity model and imposed constraints to solve temperature utilizing an enhanced genetic algorithm. Recognizing the temporal continuity of multispectral

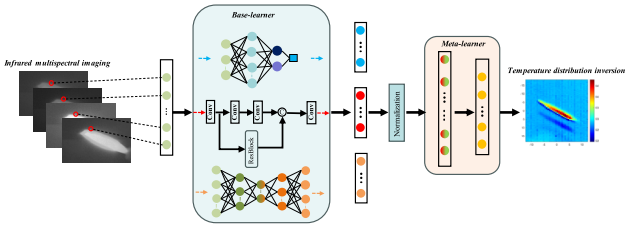

Fig. 1. Architecture of the proposed ensemble learning for temperature inversion from multispectral radiation distribution. It mainly comprises a base-learner and a meta-learner. The base-learner produces a pool of candidate base predictions. The meta-learner provides a broader receptive field for aggregation.

radiometric data, Xing *et al.* [12] proposed to employ a long short-term memory (LSTM) neural network for temperature recovery. Leveraging the feature representation ability of deep learning, Xing *et al.* [13,14] transformed one-dimensional temperature data into two-dimensional spatial data to facilitate network extraction. These pioneering investigations have introduced fresh perspectives to temperature inversion. Nevertheless, these methods employ shallow network structures, thus not fully harnessing the capabilities of deep learning, which hampers inversion accuracy and speed.

To tackle the aforementioned challenges, in this Letter, we focus on achieving precise inversion of temperature distribution in infrared multispectral imaging. We introduce ensemble learning into this problem, a novel approach to the best of our knowledge. Our network establishes a nonlinear mapping from spectral intensity measurement to temperature distribution. This mapping transforms initially inseparable data into a linearly separable form in feature space, significantly enhancing the model's regression capability. To objectively assess the performance of our method, we conduct a comparison of temperature sensing properties based on typical neural networks.

Theoretically, $\mathfrak{D} = (x_i, y_i)|i = 1, \ldots, n$ represents a multi-label training dataset, where x_i denotes the spectral radiant intensity and y_i is the corresponding temperature label. Ensemble learning aims to learn a nonlinear function h given the training dataset $\mathfrak{D}$, which maps from the radiant intensity space to subsets of temperature label space. The fundamental concept of ensemble learning is to select the most proficient base-learner for unknown emissivity and amalgamate them to achieve the final temperature inversion. As depicted in Fig. 1, we design

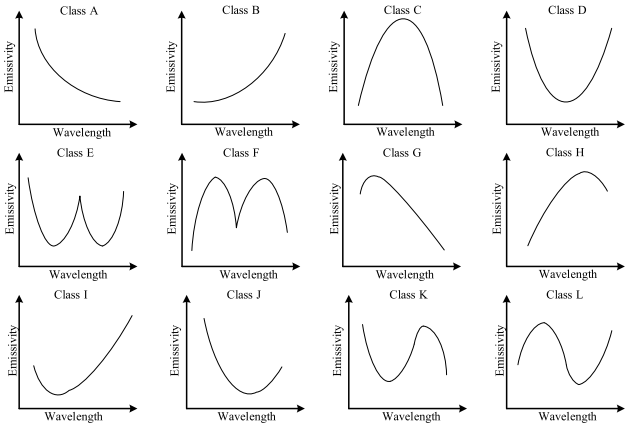

Fig. 2. Spectral emissivity diagrams for 12 class targets.

an ensemble network structure comprising a base-learner and a meta-learner. The base-learner produces a pool of candidate base predictions. To guarantee model generalization and robustness, the base-learner's construction must be precise and diverse. Building on this principle, we apply three different types of candidate networks—convolutional neural network (CNN), general regression neural network (GRNN), and BP—to predict temperature at various levels.

Before entering the meta-learner, we apply a normalization process to the initial predictions to maintain the accuracy of single predictions from the emission intensity. Consequently, the normalized initial prediction is transformed into the final label for the meta-learner. The meta-learner comprised a BP neural network with a broader receptive field for aggregation. It dynamically assigns weight relationships among base-learners, leading to enhanced inversion accuracy and model generalization.

Results and discussion. Twelve class targets with diverse emissivity trends are selected for simulation experiments, as illustrated in Fig. 2. The training temperatures range from 573 K to 1473 K, compromising 901 temperature points. At each temperature point, the 12 emissivity models are employed, resulting

Table 1. Comparisons between the Proposed and Competing Methods

Indexes	GA	BP	GRNN	RBF	ResCNN	Ours
RMSE↓	6.5732	3.8335	2.0504	9.1199	5.8743	0.9418
MAE↓	5.4893	2.8964	0.8325	7.2211	4.7214	0.4616
MdAPE↓	0.4321%	0.212%	0.020%	0.591%	0.382%	0.020%
R^2 ↑	0.9993	0.9997	0.9999	0.9987	0.9995	0.9999
MRE↓	0.673%	0.327%	0.121%	0.784%	0.527%	0.061%
Time (s)↓	6.76	0.1398	0.729	0.0871	0.0542	0.9055

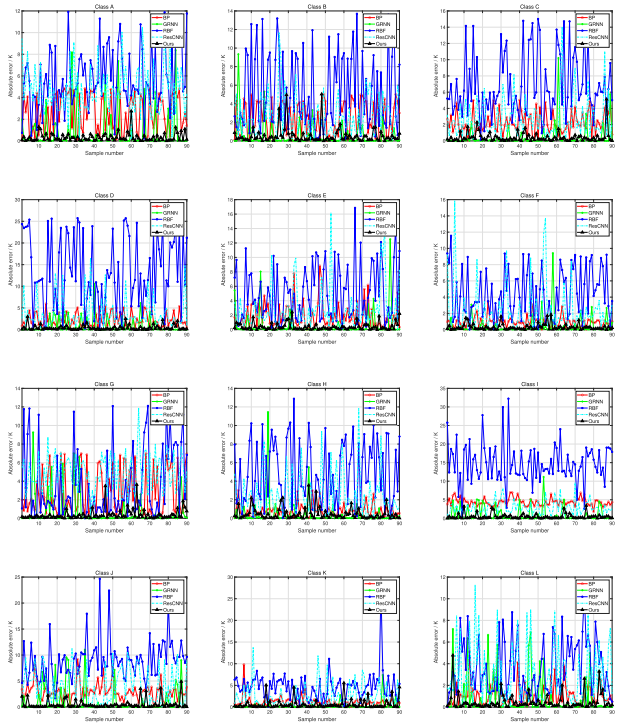

Fig. 3. Absolute errors between inversion results and ground-truth of random sampling from testing dataset among 12 class targets without noise.

in a total of 10,812 data points obtained using the Planck formula. Out of these, 9732 data points are randomly selected for network training, while 1080 data points are reserved for testing purposes. We train the network for 500 epochs with an initial learning rate of 1×10^{-2} and a batch size of 256. Our implementation is on the MATLAB R2023b with Deep Learning Toolbox, using a platform with an Intel Core i3-9100 CPU and a 16 GB RAM. Temperature inversion performance is evaluated using metrics including the root mean square error (RMSE), mean absolute error (MAE), median absolute percentage error (MdAPE), and coefficient of determination (R^2). Smaller values of MSE, RMSE, MAE, and MdAPE indicate more accurate model prediction results. The $R^2 \in [0, 1]$ assesses how well the model fits the data. A value closer to 1 signifies a better fit of the model to the data.

To demonstrate the accuracy and effectiveness of the proposed method, we compare it with one traditional optimization method and four typical neural network methods using simulation measurements. Table 1 presents the temperature inversion results on the testing dataset. It is seen that the proposed method outperforms the other competing methods. Specifically, the genetic algorithm (GA) archives good results but takes the longest running time. The RBF exhibits the largest measurement errors, while our method achieves the smallest RMSE, surpassing the second smallest value by GRNN by 1.1086. Regarding MAE, our method achieves the minimum value, nearly 45% lower than that of the suboptimal algorithm, indicating our method can more effectively avoid large prediction bias. Compared to other methods, the MdAPE and R^2 of our method and GRNN are optimally aligned, reaching 0.020% and 99.99%, respectively, demonstrating a good fit between the model and simulation data. Figure 3 illustrates the absolute errors between inversion results and ground-truth of random sampling from testing dataset of 12 class targets without noise. For most classes, the proposed method can effectively suppress the maximum absolute error, mitigating excessive inversion bias. This is attributed to the weight adjustment function of the meta-learner in the proposed method. An experiment on the noise robustness of the proposed method can be found in Supplement 1.

To validate the effectiveness of the proposed method for multispectral imaging temperature distribution inversion, we establish an infrared multispectral imaging system. As depicted in Fig. 4, it comprises six mid-wave infrared filters (3.643 μm, 3.664 μm, 3.707 μm, 4.036 μm, 4.382 μm, 4.614 μm) and a mid-wave

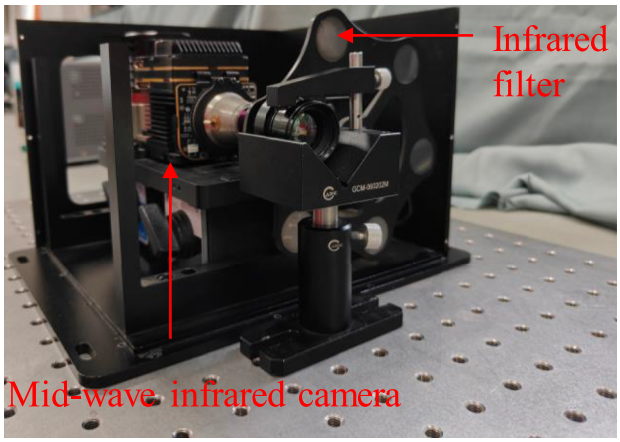

Fig. 4. Experimental platform built with the mid-wave infrared filters and camera.

Table 2. Comparison between the Inversion Temperature of Different Methods and the Blackbody Setting Temperature and the Relative Error between Them

Blackbody (K)	BP		GRNN		RBF		ResCNN		Ours	
	Inversion (K)	Relative Error	Inversion (K)	Relative Error	Inversion (K)	Relative Error	Inversion (K)	Relative Error	Inversion (K)	Relative Error
623.15	656.96	5.42%	664.30	6.60%	672.71	7.95%	635.71	2.01%	630.83	1.23%
648.15	679.74	4.87%	685.26	5.72%	699.73	7.95%	658.58	1.60%	658.79	1.64%
673.15	894.32	3.14%	693.58	3.03%	717.02	6.51%	681.59	1.25%	675.71	0.38%
698.15	711.96	1.97%	707.37	1.32%	737.34	5.61%	704.92	0.97%	697.49	0.09%
723.15	733.50	1.43%	724.86	0.23%	759.40	5.01%	730.19	0.97%	722.54	0.08%
748.15	756.80	1.15%	745.28	0.38%	783.35	4.70%	761.73	1.81%	750.81	0.35%
773.15	782.72	1.23%	767.72	0.70%	809.77	4.73%	789.57	2.12%	775.70	0.33%
798.15	808.23	1.26%	793.37	0.59%	835.67	4.70%	813.68	1.94%	798.40	0.03%
823.15	835.43	1.49%	822.51	0.07%	862.78	4.81%	852.81	3.60%	826.74	0.43%
848.15	863.74	1.49%	853.38	0.61%	886.42	4.51%	885.14	4.36%	854.55	0.75%

Table 3. Temperature Distribution Inversion by the Proposed Method on Real Thermal Targets Compared with Reference by Thermocouple

Thermal targets	Temperature (K) of P_1					Temperature (K) of P_2				
	First	Second	Third	Fourth	Reference	First	Second	Third	Fourth	Reference
Electric soldering iron	634.59	660.84	661.43	634.46	645.47	880.56	887.22	842.81	881.25	870.14
Candle flame	617.73	644.35	643.04	619.64	633.22	631.93	659.16	670.04	622.63	642.81

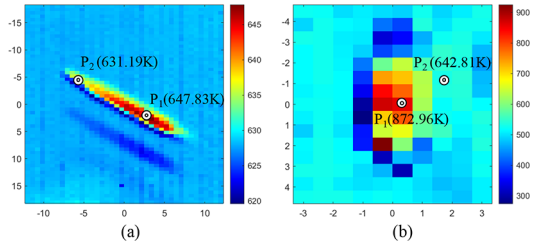

Fig. 5. Temperature distribution maps inversed by the proposed method. (a) Electric soldering iron. (b) Candle flame.

infrared camera (Gavin615A, 640 × 512). Before the actual measurement, we calibrate the spectrum and radiation response of the infrared multispectral imaging system using a monochromator and blackbody (DY-HT3, 300°–1200°, 0.1°), respectively. This ensures the accurate establishment of the corresponding relationship between the pixel gray value and incident radiation brightness.

Table 2 presents a comparison between the inversion temperature obtained from different methods and the blackbody setting temperature, along with their relative errors. It is noted that when the blackbody temperature exceeds 900 K, the infrared radiation exceeds the dynamic response range of the mid-wave infrared camera, resulting in an overexposure effect on the camera, which cannot obtain effective radiation values for temperature inversion. It is observed that compared to other competing methods, the relative error of GRNN exceeds 1% below 700 K, indicating a suboptimal performance. Additionally, apart from 823.15 K and 848.15 K, the proposed method achieves the highest accuracy in temperature inversion.

In order to further explain the effect of the proposed method on temperature distribution inversion, we conduct additional experiments using real thermal targets, including an electric soldering iron and a candle. The measurement results of thermocouple are used as reference. The temperature distribution maps inversed by the proposed method are displayed in Fig. 5, where the temperatures of two selected points P_1 and P_2 are shown in Table 3. It is seen that the proposed method provides accurate temperature distribution inversion.

This Letter introduces a novel approach to temperature distribution inversion in infrared multispectral imaging, leveraging ensemble learning. Ensemble learning is preliminarily utilized to establish nonlinear mapping from spectral intensity measurement to temperature distribution. A meticulously designed base-learner generates preliminary sensing data, which is then aggregated by a meta-learner for temperature inversion. As a result, the proposed method demonstrates promising inversion accuracy and model generalization. Extensive simulation experiments on 12 class targets, including 1% noise, reveal that the proposed method achieves a minimum error of 0.02 K and a maximum error of 6.10 K, outperforming algorithms implemented by some typical neural networks. This property of robustness is of great significance for practical applications. Furthermore, we establish an experimental platform based on infrared multispectral imaging, accurately inverting the temperature distribution of real thermal targets from the multispectral measurement. However, the traditional multispectral imaging system is bulky, so the joint optimization of system and inversion algorithm will be studied in the future to realize the temperature distribution inversion on-chip.

Funding. Shaanxi Province Postdoctoral Project (2023BSHEDZZ163); Xian City Science and Technology Plan Project (21JBGSZ-QCY9-0004, 22JBGS-QCY4-0006, 23GBGS0001, 23ZDCYJSGG0011-2023); Ministry of Universities (Spain) (FPU2020-05532); Aeronautical Science Foundation of China (20230024081027); Shaanxi Province Science and Technology Plan Project (2023KXJ-170); Shaanxi Province Key Research and Development Plan Project (2022JBGS209).

Disclosures. The authors declare no conflicts of interest.

Data availability. Data underlying the results presented in this Letter are not publicly available at this time but may be obtained from the authors upon reasonable request.

Supplemental document. See Supplement 1 for supporting content.

REFERENCES

1. N. J. Kempema and M. B. Long, Opt. Lett. **43**, 1103 (2018).
2. K. Ridier, A.-C. Bas, Y. Zhang, *et al.*, Nat. Commun. **11**, 3611 (2020).
3. T. Liu and A. Fiore, Optica **7**, 934 (2020).
4. Z. Hayran, A. Chen, and F. Monticone, Optica **8**, 1040 (2021).
5. B. Sun, X. Sun, and J. Dai, Results Phys. **19**, 103388 (2020).
6. J. Xing, W. Sun, X. Sun, *et al.*, Part. Part. Syst. Charact **29**, 16 (2012).
7. J. Xing, B. Peng, Z. Ma, *et al.*, Opt. Express **25**, 30560 (2017).
8. Z. Zhao, D. Chen, J. Dong, *et al.*, Opt. Lett. **49**, 957 (2024).
9. D. Cong and J. Dai, J. Infrar. Milli. Waves **20**, 97 (2001).
10. X. Sun, G. Yuan, and J. Dai, Guang Pu Xue Yu Guang Pu Fen Xi **27**, 213 (2007).
11. L. Chen, S. Sun, S. Gao, *et al.*, Infrared Phys. Technol. **111**, 103523 (2020).
12. J. Xing, P. Yan, W. Li, *et al.*, Opt. Express **30**, 46081 (2022).
13. N. Zhang, J. Xing, and S. Cui, Opt. Express **31**, 38038 (2023).
14. J. Xing, J. Guo, S. Cui, *et al.*, Opt. Lett. **48**, 2166 (2023).